Accelerated Uplift and Magmatic Intrusion of the Yellowstone Caldera, 2004 to 2006

Wu-Lung Chang, *et al.*

Science **318**, 952 (2007);
DOI: 10.1126/science.1146842

Science (print ISSN 0036-8075; online ISSN 1095-9203) is published weekly, except the last week in December, by the American Association for the Advancement of Science, 1200 New York Avenue NW, Washington, DC 20005.

(*20*, *25*). The angles $\Phi_{e-e} = 90°$ and $\Phi_{e-e} = -90°$ correspond to a kick of the second electron, either to the left or the right. This strong electron-electron Coulomb interaction mediates the double ionization and creates an entanglement between the two electrons. Electron collisions of this sort in bound systems have been demonstrated directly in pump-probe experiments (*26*).

This situation is an intramolecular version of a scattering event downstream of a double slit (*27*, *6*). When either photons (*6*) or particles (*27*) are scattered from a beam after passage through a double slit, the scattering induces a phase shift, which then leads to a shift of the interference pattern. If the momentum transfer is not measured in coincidence (*6*), the fringe visibility is lost. In this experiment, both electrons are initially delocalized inside the molecule in a completely coherent single quantum state. Before photoabsorption, both electrons are confined in the hydrogen ground state, which is symmetric with respect to its two atomic centers. Thus, we observed not a scattering between classical localized particles but a coherent entanglement of the wave function of the two electrons.

It is instructive to think of the electronic two-body system as split into its subsystems and to consider one subsystem as the environment of the other. The strong Coulomb interaction entangles the two subsystems and leads to a position-dependent modification of phase of the single-particle wave function inside each of the two subsystems. The entanglement of the electrons in the pair is directly visible in their mutual angular distribution and is further evidenced by the observation that selecting the momentum of one electron makes the interference pattern of its partner reappear. In the spirit of discussions dating from the early history of quantum mechanics, one particle can be considered an observer that carries partial information about the other particle and its path through the double slit. The amount of which-way information exchanged between the particles is limited by the observer particle's de Broglie wavelength (*28*). The key difference between the situation depicted in Fig. 2A (which shows interference) and Fig. 2B (which shows no interference) is that the wavelength of the second, unobserved electron is much shorter in the latter case.

Our experiment thus reveals that a very small number of particles suffices to induce the emergence of classical properties, such as the loss of coherence. A four-body system, such as fragmented molecular hydrogen, acts as a double slit in the sense that coherence is lost in a subsystem of entangled electrons. Such a fundamental system facilitates the study of the influence of interelectronic Coulomb interactions on the coherence properties of a single electron. In solid-state–based quantum computing devices, such electron-electron interaction represents a key challenge. One advantageous aspect of the finite system investigated here is that, theoretically, it is fully tractable at present (*29*–*32*).

References and Notes

1. C. Jönnson, *Z. Phys. A* **161**, 454 (1961).
2. M. Arndt *et al.*, *Nature* **401**, 680 (1999).
3. M. Noel, C. Stroud, *Phys. Rev. Lett.* **75**, 1252 (1995).
4. E. Joos, H. Zeh, *Z. Phys. B* **59**, 223 (1985).
5. W. Zurek, *Rev. Mod. Phys.* **75**, 715 (2003).
6. D. A. Kokorowski, A. D. Cronin, T. D. Roberts, D. E. Pritchard, *Phys. Rev. Lett.* **86**, 2191 (2001).
7. L. Hackermüller, K. Hornberger, B. Brezger, A. Zeilinger, M. Arndt, *Nature* **427**, 711 (2004).
8. H. Cohen, U. Fano, *Phys. Rev.* **150**, 30 (1966).
9. D. Rolles *et al.*, *Nature* **7059**, 711 (2005).
10. X. Liu *et al.*, *J. Phys. B* **39**, 4801 (2006).
11. I. Kaplan, A. Markin, *Sov. Phys. Dokl.* **14**, 36 (1969).
12. M. Walter, J. Briggs, *J. Phys. B* **32**, 2487 (1999).
13. J. Fernandez, O. Fojon, A. Palacios, F. Martín, *Phys. Rev. Lett.* **98**, 043005 (2007).
14. N. Stolterfoht *et al.*, *Phys. Rev. Lett.* **87**, 023201 (2001).
15. D. Misra *et al.*, *Phys. Rev. Lett.* **92**, 153201 (2004).
16. J. Ullrich *et al.*, *Rep. Prog. Phys.* **66**, 1463 (2003).
17. R. Dörner *et al.*, *Phys. Rep.* **330**, 95 (2000).
18. O. Jagutzki *et al.*, *Nucl. Instrum. Methods A* **477**, 244 (2002).
19. T. Weber *et al.*, *Nature* **431**, 437 (2004).
20. A. Knapp *et al.*, *Phys. Rev. Lett.* **89**, 033004 (2002).
21. G. L. Yudin, S. Chelkowski, A. D. Bandrauk, *J. Phys. B* **39**, L17 (2006).
22. S. K. Semenov, N. A. Cherepkov, *J. Phys. B* **36**, 1409 (2003).
23. R. Díez Muiño, D. Rolles, F. J. García de Abajo, C. S. Fadley, M. A. Van Hove, *J. Phys. B* **35**, L359 (2002).
24. T. Opatrny, G. Kurizki, *Phys. Rev. Lett.* **86**, 3180 (2001).
25. M. Pont, R. Shakeshaft, *Phys. Rev. A* **51**, R2676 (1995).
26. S. N. Pisharody, R. R. Jones, *Science* **303**, 813 (2004).
27. K. Hornberger *et al.*, *Phys. Rev. Lett.* **90**, 160401 (2003).
28. W. Wootters, W. Zurek, *Phys. Rev. D* **19**, 473 (1979).
29. W. Vanroose, F. Martín, T. Rescigno, C. W. McCurdy, *Science* **310**, 1787 (2005).
30. F. Martín *et al.*, *Science* **315**, 629 (2007).
31. J. Colgan, M. S. Pindzola, F. Robicheaux, *J. Phys. B* **37**, L377 (2004).
32. D. Dundas, *J. Phys. B* **37**, 2883 (2004).

33. We thank M. Walter, J. Briggs, A. Kheifets, U. Becker, D. Rolles, E. Joos, K. Ueda, M. Arndt, and M. Aspelmeyer for enlightening discussions. We acknowledge outstanding support by the staff of the Advanced Light Source, in particular by E. Arenholz, T. Young, H. Bluhm, and T. Tyliszczak. This work was supported by the Deutsche Forschungsgemeinschaft and by the Office of Basic Energy Sciences, Division of Chemical Sciences of the U. S. Department of Energy under contract DE-AC03-76SF00098.

10 May 2007; accepted 18 September 2007
10.1126/science.1144959

Accelerated Uplift and Magmatic Intrusion of the Yellowstone Caldera, 2004 to 2006

Wu-Lung Chang,[1]* Robert B. Smith,[1]* Charles Wicks,[2] Jamie M. Farrell,[1] Christine M. Puskas[1]

The Yellowstone caldera began a rapid episode of ground uplift in mid-2004, revealed by Global Positioning System and interferometric synthetic aperture radar measurements, at rates up to 7 centimeters per year, which is over three times faster than previously observed inflation rates. Source modeling of the deformation data suggests an expanding volcanic sill of ~1200 square kilometers at a 10-kilometer depth beneath the caldera, coincident with the top of a seismically imaged crustal magma chamber. The modeled rate of source volume increase is 0.1 cubic kilometer per year, similar to the amount of magma intrusion required to supply the observed high heat flow of the caldera. This evidence suggests magma recharge as the main mechanism for the accelerated uplift, although pressurization of magmatic fluids cannot be ruled out.

The Yellowstone volcanic field is the largest in North America (Fig. 1A). The youngest of three giant eruptions that formed the field occurred 640,000 years ago, creating the 40-km-wide by 60-km-long Yellowstone caldera. This eruption was followed by 30 smaller eruptions of dominantly rhyolite flows, the youngest 70,000 years ago (*1*). Earthquakes, ground deformation, very high heat flow, and the world's largest distribution of hydrothermal features characterize Yellowstone (*2*, *3*), similar to those of other silicic volcanic fields such as Long Valley, California, and Phlegrean Fields, Italy (*4*, *5*).

Geodetic measurements of Yellowstone from 1923 to 2004 using precise leveling, GPS (Global Positioning System), and InSAR (interferometric synthetic aperture radar) have revealed multiple episodes of caldera uplift and subsidence, with maximum average rates of ~1 to 2 cm/year generally centered at its two resurgent domes, Sour Creek and Mallard Lake (*6*–*8*). In addition, an area northwest of the caldera near Norris Geyser Basin experienced periods of substantial ground deformation (*8*, *9*). These spatial and temporal variations of the Yellowstone unrest also correlated with pronounced changes in seismic and hydrothermal activity (*9*, *10*) (Fig. 1B).

[1]Department of Geology and Geophysics, University of Utah, Salt Lake City, UT 84112, USA. [2]U.S. Geological Survey, MS 977, Menlo Park, CA 94025, USA.

*To whom correspondence should be addressed. E-mail: wchang@earth.utah.edu (W.-L.C.); R.Smith@earth.utah.edu (R.B.S.)

The University of Utah and the Plate Boundary Observatory (PBO) operate twelve continuous-recording GPS stations in Yellowstone to monitor ground movement (*11*) (Fig. 1A). Temporal variations of the vertical deformation (Fig. 2A) show 1 to 2 cm of subsidence in the caldera (e.g., at station LKWY) and uplift in the Norris area (at station NRWY) during the first 6 months of 2004. The caldera motion then suddenly reversed to uplift in July 2004 at unexpected high rates, ~7 cm/year at station WLWY, whereas the Norris area began to subside about 3 months later. Accelerated horizontal movements correlated in time with the changes in vertical motions (fig. S1). The GPS data also reveal a near-simultaneous inception of uplift across the entire caldera (Fig. 2A), in contrast to the previous observations that deformation shifted laterally from the Sour Creek dome toward the Mallard Lake dome in 1 to 2 years (*7*).

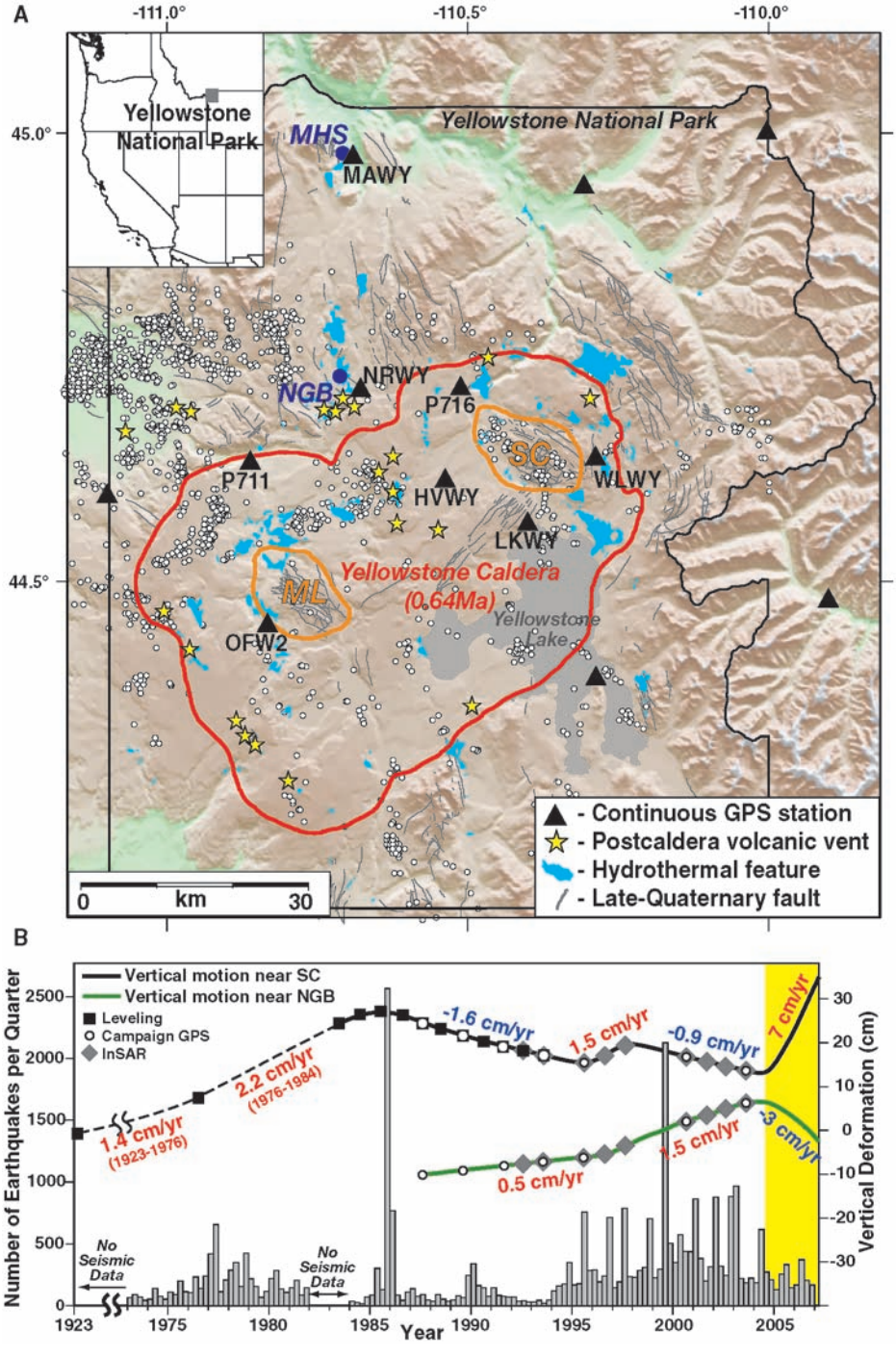

Fig. 1. (**A**) Volcano tectonic setting and GPS station locations of the Yellowstone volcanic field. White circles are earthquake epicenters from October 2004 to March 2007. SC indicates Sour Creek resurgent dome; ML, Mallard Lake resurgent dome; NGB, Norris Geyser Basin; and MHS, Mammoth Hot Springs. GPS station names are abbreviated to four-character codes. Ma, million years ago. (**B**) Time sequence of Yellowstone vertical ground motions and quarterly earthquake counts. Different symbols represent early geodetic measurements (*6*–*9*). The yellow shaded area highlights the period of accelerated deformation reported in this study. Note that the 1923–1976 and 1976–1984 rates were each determined from only two measurements.

InSAR measurements (ENVISAT IS1 and IS2 modes) from 2004 to 2006 (*11*), with a spatial resolution of ~30 m, reveal ground motions that are consistent with the GPS observations (Fig. 2B and fig. S2). The inflation increases symmetrically toward the caldera center about the long axis (northeast-southwest), with the highest rate of ~7 cm/year at the Sour Creek dome being three to five times faster than uplift rates in 1923–1984 and 1995–1997 (Fig. 1B). The Norris subsidence is ~3 cm/year, more than two times greater than the 1996–2002 uplift rate in this area. The GPS horizontal velocities, in addition, indicate ground motions directed outward from the caldera at 0.8 to 2.2 cm/year and inward to the Norris area at 0.7 to 2.0 cm/year.

To evaluate the causes of the observed rapid deformation, we jointly inverted the GPS and InSAR data (*12*) for the geometry and expansion or contraction of rectangular dislocations in a homogeneous elastic half-space to simulate inflating and deflating volcanic volumes. A nonlinear optimization method was used to determine the source model that minimizes the difference between the observed and predicted ground motions (*13*). Uncertainties of model parameters were evaluated by a χ^2 method (*11*).

The best-fitting sources for the GPS and IS2 InSAR data include an expanding sill-like volume dipping 5°SE (5°NW to 15°SE) at a depth of 10 km (6 to 14 km) beneath the Yellowstone caldera and a contracting volume dipping 12°SE (7°NW to 18°SE) at a depth of 8 km (6 to 16 km) under the Norris area (Fig. 3). The average rates of volumetric change are 0.11 km^3/year (0.10 to 0.12 km^3/year) and –0.01 km^3/year (–0.005 to –0.015 km^3/year) for the inflating and deflating sources, respectively. A joint inversion of the GPS and IS1 InSAR data also resulted in similar source parameters, indicating the robust nature of the modeling results (fig. S3). Our models, assuming uniform constitutive properties, predict ~90% of the observed ground motion within the data confidence limits. We also tested the effects of crustal heterogeneity by including layers with different elastic constants and showed that they would not notably affect our modeling results (*11*).

Episodic intrusion or recharge of magma into the upper crust has been proposed as a mechanism for previous Yellowstone caldera uplift (*1*, *2*). In this conceptual model, basaltic

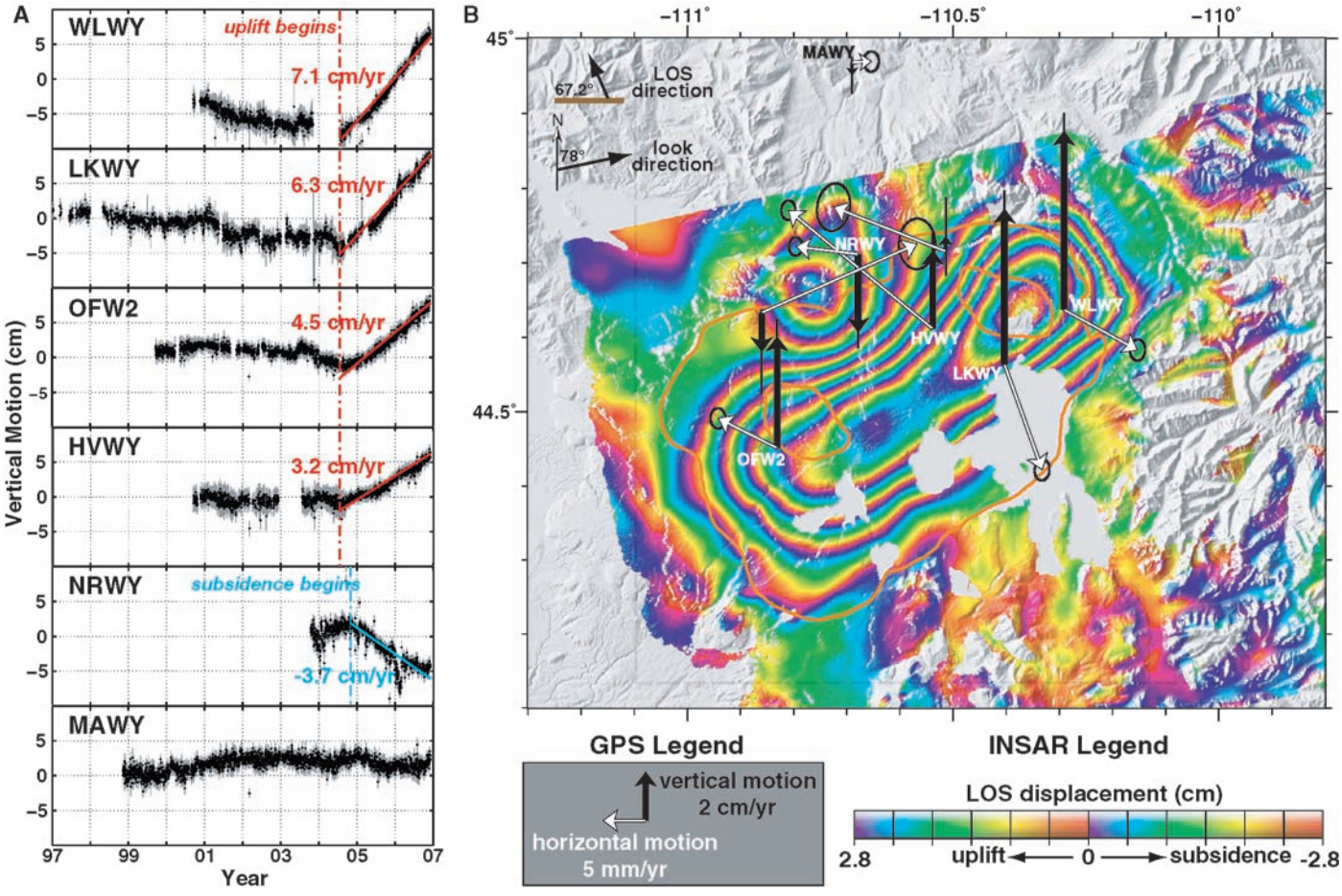

Fig. 2. (**A**) Temporal variation of vertical ground motions of labeled Yellowstone GPS stations. Each dot represents a daily position determination. Light gray bars are 1-σ errors. Red and blue dot-dash lines mark the inceptions of the uplift and the subsidence, respectively. Deformation rates are the slopes of the interpolated lines. (**B**) A stacked InSAR interferogram (ENVISAT IS2 mode) from 22 September 2004 to 23 August 2006 overlain with averaged GPS velocities from 07 October 2004 and 07 October 2006. The line-of-sight (LOS) displacement of Earth's surface toward the satellite from the interferogram infers a total uplift of about 11 cm in the west part of the caldera and as large as 15 cm at the Sour Creek resurgent dome and a subsidence of 6.6 cm near the Norris Geyser Basin. White and black arrows represent horizontal and vertical velocity vectors, respectively. Black ellipses and bars are scaled 2-σ errors (*11*).

magma originating from a mantle plume at depths of ~50 km ascends buoyantly through the crust, providing thermal energy to partially melt crustal rocks and create the rhyolitic magma component that characterizes the silicic volcanism. The basaltic and rhyolitic magmas then crystallize and cool, releasing energy responsible for Yellowstone's extraordinarily high heat flow of ~2000 mW/m^2 measured from Yellowstone Lake (*14*) and geochemical evidence (*3*).

Seismic tomographic imaging provided direct evidence for the partially molten crustal magma chamber beneath the caldera (*15*). Anomalies of low P-wave velocity, up to 6%, at depths of 8 to 16 km were interpreted as a body of crystallized magma of ~4000 km^3 directly underlying the caldera. The top of this body and our modeled sill overlap (Fig. 3E), implying that the accelerated uplift is caused by inflation from the shallow part of the magma chamber. Moreover, to maintain the observed caldera heat flux requires a magma crystallization rate of ~0.1 km^3/year (*3*), which is comparable to our modeled source expansion rate.

We thus suggest that the 2004–2006 episode of accelerated inflation occurred in response to a caldera-wide magma recharge of the Yellowstone volcanic system. Such a high rate of intrusion may have occurred during past uplift episodes, for example between the first two leveling surveys in 1923 and 1976, when the caldera rose a total of ~75 cm but the rate of 1.4 cm/year was linearly interpolated between observations (Fig. 1B).

An alternate interpretation for the caldera uplift is that magmatic fluids (water and gases) exsolved from magma crystallization were trapped beneath impermeable rocks, causing pressurization of the deep hydrothermal system and in turn inflating the ground surface (Fig. 4). Crystallizing 0.1 km^3/year of rhyolitic magma, which is required to provide the observed thermal heat flow, and trapping all the released water would result in a volumetric expansion of ~0.013 km^3/year (*3*, *16*). This value, however, is about 10 times smaller than the source inflation rate of 0.11 km^3/year responsible for the current uplift. Although the volumetric expansion could be greater if gas discharge is taken into account, this mechanism requires a rapid increase in fluid exsolution from magma crystallization to account for the accelerated caldera uplift and is thus a less viable cause for the observed deformation.

Source modeling of early episodes of caldera inflation (*7*, *17*) imply geometries and depths similar to those from our model but much lower rates of volumetric increase, 0.01 to 0.03 km^3/year, which are comparable to the rates from the above magmatic fluid model. This evidence suggests that pressurizing fluid systems near the top of the crustal magma reservoir is a plausible source mechanism for the previous uplift episodes. Therefore, magma intrusion and fluid pressurization should be considered as jointly operating processes to explain the accelerated caldera uplift reported here, although our estimate of large volume increase implies the former as a preferred source model. Further independent observations, such as temporal microgravity changes, capable of resolving mass and density variations of the magmatic reservoir would be useful to discrim-

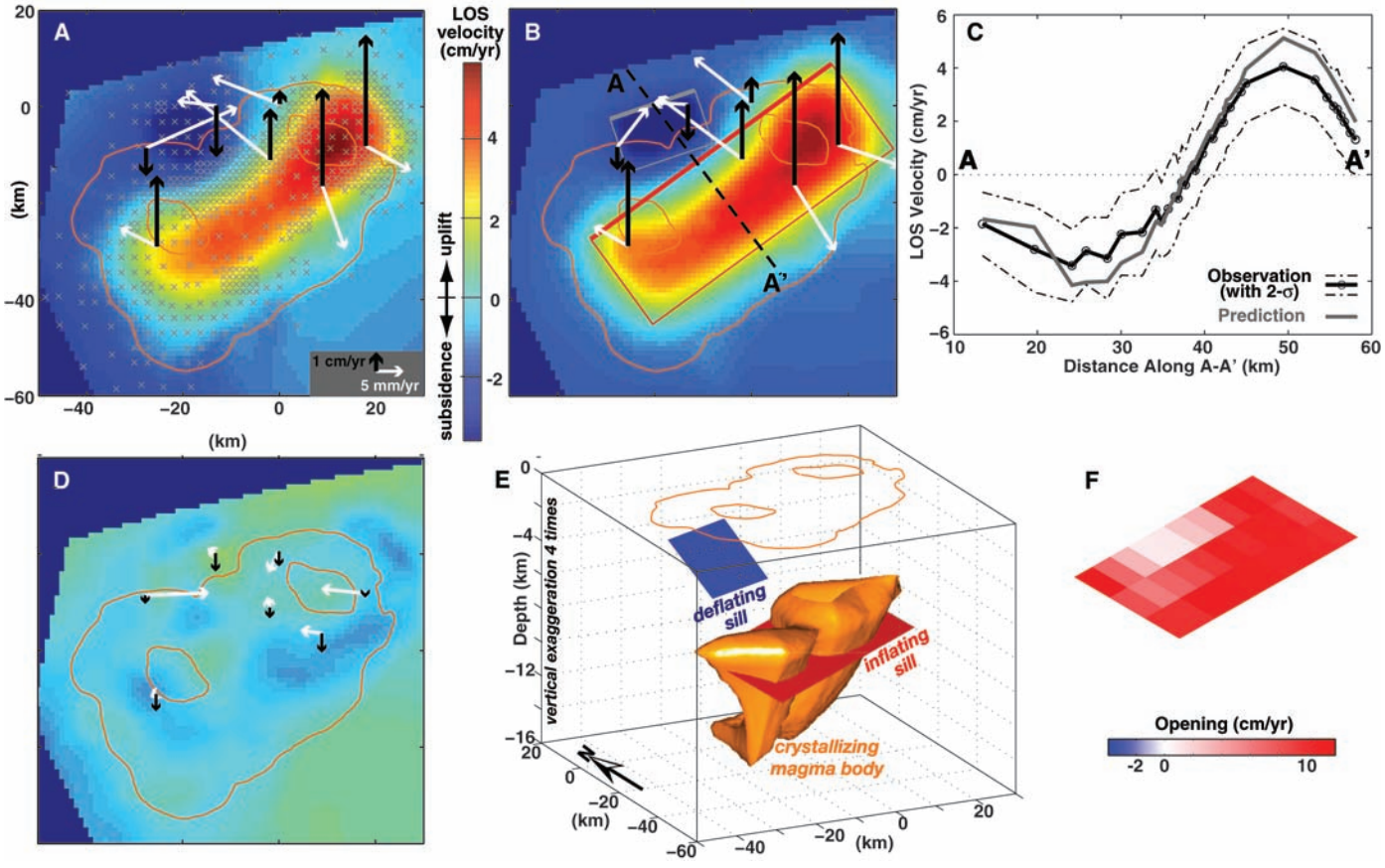

Fig. 3. (**A**) Observed Yellowstone ground motion, 2004–2006. Black and white arrows are vertical and horizontal velocity vectors, respectively, measured by GPS. Background colors represent average LOS velocities interpolated by reduced InSAR data points (gray crosses) (*11*). (**B**) Modeled ground motion. Surface projections of the modeled expanding and contracting sills are shown by red and gray rectangles, respectively. Solid lines highlight the tops of the sills. (**C**) Modeled and observed ground motion along the profile A-A′ in (B). (**D**) Residuals between data and model predictions. (**E**) Three-dimensional view (from the southwest) of the modeled volcanic sills superimposed on a seismically imaged magma body (*15*). (**F**) Opening distribution of the modeled inflating sill. We first assumed a uniform dislocation beneath the caldera to solve for the geometry of the sill. The dislocation was then discretized into 30 patches, and the opening of each was estimated to best explain the spatial variation of the caldera uplift (*11*).

inate the contribution between the two different volcanic mechanisms (*18*, *19*).

The inflation of the magmatic sill can induce dilatational strain in the surrounding volcanic rocks (Fig. 4), leading to an increase in permeability and a decrease in pore pressure by opening new or self-sealed fractures. Accordingly, the dilated zone beneath the northern caldera can experience lower pore pressure relative to the hydrothermal reservoirs beneath the Norris area. This induced pressure gradient can thereby drive fluids southeastward into the caldera, depressurizing the Norris hydrothermal systems and causing the ground there to subside. Previous studies also implied that the widespread hydrothermal and volcanic features across the northern caldera boundary indicate highly fractured and permeable crustal rocks, providing pathways for fluid migration (*9*, *16*).

We therefore propose that the 2004–2006 deflation near Norris Geyser Basin was in response to a redistribution of hydrothermal fluids as a consequence of caldera inflation. Moreover, earthquake activity during the deformation period was concentrated near the northern caldera boundary, while the rest of the caldera experienced low rates of seismicity (Fig. 1A). Volumetric expansion of crustal rocks due to the induced dilatation can increase the strain rate and promote brittle fracturing. With fluids migrating from the Norris region into the caldera, earthquakes can be induced within the dilated zone between the inflating and deflating source volumes (Fig. 4).

The caldera-wide accelerated uplift reported here is interpreted as magmatic recharge of the Yellowstone magma body (*20*). Although the geodetic observations and models do not imply an impending volcanic eruption or hydrothermal explosion, they are important evidence of ongoing processes of a large caldera that was produced by a super volcano eruption.

References and Notes

1. R. L. Christiansen, *U.S. Geol. Surv. Prof. Pap. 729-G* (2001).
2. R. B. Smith, L. W. Braile, *J. Volcanol. Geotherm. Res.* **61**, 121 (1994).
3. R. O. Fournier, *Annu. Rev. Earth Planet. Sci.* **17**, 13 (1989).
4. D. P. Hill, *Geol. Soc. London Spec. Publ.* **269**, 1 (2006).
5. G. De Natale *et al.*, *Geol. Soc. London Spec. Publ.* **269**, 25 (2006).
6. D. Dzurisin, K. M. Yamashita, J. W. Kleinman, *Bull. Volcanol.* **56**, 261 (1994).
7. C. Wicks, W. Thatcher, D. Dzurisin, *Science* **282**, 458 (1998).
8. C. M. Puskas, R. B. Smith, C. M. Meertens, W. L. Chang, *J. Geophys. Res.* **112**, 10.1029/2006JB004325 (2007).
9. C. Wicks, W. Thatcher, D. Dzurisin, J. Svarc, *Nature* **440**, 72 (2006).
10. G. P. Waite, R. B. Smith, *J. Geophys. Res.* **107**, 10.1029/2001JB000586 (2002).
11. Materials and methods are available as supporting material on *Science* Online.
12. After several tests we chose to weigh the GPS velocity measurements by a factor of 5 to equal the contribution of the GPS and InSAR data sets to the inversion.
13. P. Cervelli *et al.*, *J. Geophys. Res.* **107**, 10.1029/2001JB000602 (2002).
14. P. Morgan, D. D. Blackwell, R. E. Spafford, R. B. Smith, *J. Geophys. Res.* **82**, 3719 (1977).
15. S. Husen, R. B. Smith, G. P. Waite, *J. Volcanol. Geotherm. Res.* **131**, 397 (2004).
16. D. Dzurisin, J. C. Savage, R. O. Fournier, *Bull. Volcanol.* **52**, 247 (1990).
17. D. W. Vasco, C. M. Puskas, R. B. Smith, C. M. Meertens, *J. Geophys. Res.* **112**, 10.1029/2006JB004641 (2007).
18. M. Battaglia, C. Roberts, P. Segall, *Science* **285**, 2119 (1999).

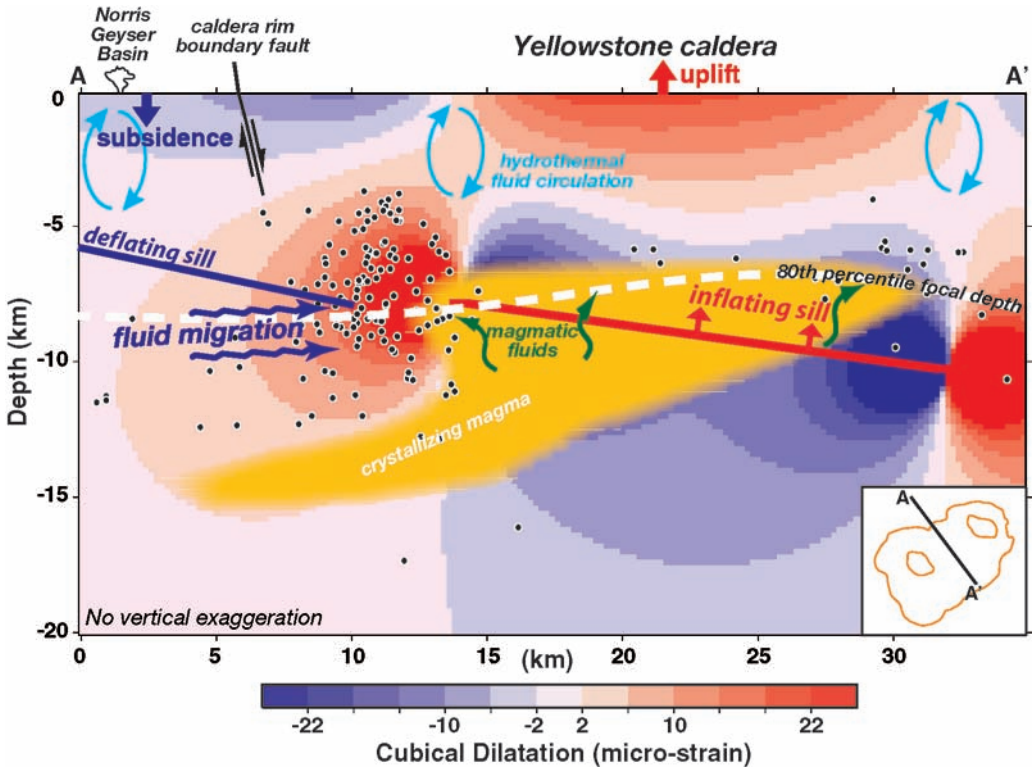

Fig. 4. Schematic diagram of plausible magmatic and hydrothermal processes responsible for 2004–2006 accelerated Yellowstone caldera uplift and Norris subsidence. Black dots are earthquake hypocenters from October 2004 to March 2007 (see Fig. 1A for the epicenters). The yellow area shows the seismically imaged magma body in Fig. 3E. Background colors represent cubical dilatation, in unit changes of volume, induced by the modeled inflating sill. Fluids exsolved from magma crystallization can be trapped beneath the nonpermeable rocks near the brittle-ductile transition zone, taken as the 80th percentile focal depth of earthquakes (white dashed line) (*21*, *22*), to produce the caldera uplift.

19. J. Gottsmann, A. Folch, H. Rymer, *J. Geophys. Res.* **111**, 10.1029/2005JB003745 (2006).
20. Updated GPS data show that this episode of Yellowstone caldera uplift is continuing as of September 2007 (fig. S1).
21. R. B. Smith, R. L. Bruhn, *J. Geophys. Res.* **89**, 5733 (1984).
22. S. Husen, R. B. Smith, *Bull. Seismol. Soc. Am.* **94**, 880 (2004).

23. This project has been a cooperative effort of the University of Utah, the Yellowstone Volcano Observatory, and the EarthScope PBO. ENVISAT data were provided by the European Space Agency as part of Cat-1 project 2765. Discussions with R. Fournier, C. Meertens, G. Waite, H. Heasler, and J. Lowenstern greatly benefited the paper. M. Poland, S.-H. Yun, and three anonymous reviewers provided constructive comments. The research was funded by the NSF Continental Dynamics Program, grant no. EAR0314237, and The Brinson Foundation.

Supporting Online Material
www.sciencemag.org/cgi/content/full/318/5852/952/DC1
Materials and Methods
Figs. S1 to S3
Tables S1 and S2
References and Notes

21 June 2007; accepted 4 October 2007
10.1126/science.1146842

Observation of the One-Dimensional Diffusion of Nanometer-Sized Dislocation Loops

K. Arakawa,[1]* K. Ono,[2] M. Isshiki,[3] K. Mimura,[3] M. Uchikoshi,[3] H. Mori[1]

Dislocations are ubiquitous linear defects and are responsible for many of the properties of crystalline materials. Studies on the glide process of dislocations in bulk materials have mostly focused on the response of dislocations with macroscopic lengths to external loading or unloading. Using in situ transmission electron microscopy, we show that nanometer-sized loops with a Burgers vector of ½⟨111⟩ in α-Fe can undergo one-dimensional diffusion even in the absence of stresses that are effective in driving the loops. The loop size dependence of the loop diffusivity obtained is explained by the stochastic thermal fluctuation in the numbers of double kinks.

The hardness and toughness of crystalline materials is often governed by the generation and motion of linear defects termed dislocations (*1*). Previous studies on the glide process of dislocations in bulk materials have focused on the response of dislocations with macroscopic lengths to external loading or unloading (*1*, *2*). On the other hand, it is known that nanoscale dislocations can be formed as loops in bulk materials by the agglomeration of self-interstitial atoms, which are produced upon energetic particle irradiation, in the shape of disks. Recent molecular dynamics (MD) calculations have shown that in metals and alloys, extremely small interstitial-type dislocation loops with diameters of less than a few nanometers can undergo fast one-dimensional (1D) glide diffusion in the direction of their Burgers vector, **b**, even under zero stress (*3*–*7*). This phenomenon has also been examined theoretically (*8*–*10*). Other computational and theoretical studies have shown that the loop diffusion plays a central role in the degradation processes of materials for nuclear fission and nuclear fusion, upon high-energy particle irradiation (*11*, *12*).

One MD study has shown that the highly diffusive loops with **b** values of ½[111] in α-Fe, which are smaller than ~2.4 nm in diameter, can be regarded as bundles of crowdions with [111] axes (*6*). A crowdion is a kind of a self-interstitial atom (*13*); it has a long-range compression-strain field in a close-packed direction, and its center of mass can easily move one-dimensionally along the axis. The crowdion bundles move by the almost independent motions of the constituent crowdions along their

[1]Research Center for Ultra-High Voltage Electron Microscopy, Osaka University, 7-1 Mihogaoka, Ibaraki, Osaka 567-0047, Japan. [2]Department of Material Science, Shimane University, 1060 Nishikawatsu, Matsue 690-8504, Japan. [3]Institute of Multidisciplinary Research for Advanced Materials, Tohoku University, 2-2-1 Katahira, Aoba-ku, Sendai 980-8577, Japan.

*To whom correspondence should be addressed. E-mail: arakawak@uhvem.osaka-u.ac.jp